Materials Science, Vol. 21, No. 2, 2003

Spin-entropy driven charge-transfer phase transition in iron mixed-valence system*

N. KOJIMA**, M. ITOI, Y. ONO, M. OKUBO, M. ENOMOTO

Graduate School of Arts and Sciences, The University of Tokyo, Tokyo 153-8902, Japan

We have synthesized iron mixed-valence complexes, $(n\text{-}C_nH_{2n+1})_4N[Fe^{II}Fe^{III}X_3]$ (X = mto (C_2O_3S), dto ($C_2O_2S_2$), tto (C_2OS_3)) and have investigated their physical properties by means of ^{57}Fe Mössbauer spectroscopy, magnetic susceptibility and electrical resistivity measurements. From the analysis of ^{57}Fe Mössbauer spectra, magnetic susceptibility and electrical resistivity, we have discovered a new type of first order phase transition around 120 K for $(n\text{-}C_nH_{2n+1})_4N[Fe^{II}Fe^{III}(dto)_3]$ (n = 3, 4), where the charge-transfer transition between Fe^{II} and Fe^{III} occurs reversibly. In the higher temperature phase, the Fe^{III} (S = 1/2) and Fe^{II} (S = 2) sites are co-ordinated by six S atoms and six O atoms, respectively. In the lower temperature phase, on the other hand, the Fe^{III} (S = 5/2) and Fe^{II} (S = 0) sites are co-ordinated by six O atoms and six S atoms, respectively. Moreover, we have found a ferromagnetic phase transition in this system. The ferromagnetic order is induced by the charge-transfer interaction between the Fe^{III} and Fe^{II} sites. We propose various multifunctional properties for $(n\text{-}C_nH_{2n+1})_4N[Fe^{II}Fe^{III}(mto)_3]$ and $(n\text{-}C_nH_{2n+1})_4N[Fe^{II}Fe^{III}(tto)_3]$.

Key words: *spin crossover; ferromagnetism; charge-transfer; phase transition; mixed valence*

1. Introduction

Transition metal complexes with d^4-d^7 configuration have a possibility of spin transition between a low-spin state and a high spin state. The spin crossover phenomenon has recently gained renewed importance since the discovery of the photo-induced spin transition (called LIESST = Light Induced Excited Spin State Trapping) for $[Fe(ptz)_6](BF_4)_2$(ptz = 1-propyltetrazole) [1] and the thermally induced spin crossover transition with large thermal hysteresis around room temperature for a triazole bridged iron(II) complex [2, 3]. In the case of assembled hetero-metal complex system including spin-crossover complex ion, the spin transition behaves as a switching

---

* The paper was presented at the 13th Winter School on Coordination Chemistry, Karpacz, Poland, 9–13 December, 2002.

** Corresponding author, e-mail: cnori@mail.ecc.u-tokyo.ac.jp.

function to amplify the magnetic dimensionality, the magnetic interaction and to induce the magnetic ordering, which is schematically shown in Fig. 1.

In the spin-crossover system, the enthalpy term (*H*) dominates the Gibbs free energy ($G = H - TS$) in the low-spin state, while the entropy term ($-TS$) dominates the free energy in the high-spin state. Usual spin-crossover phenomenon occurs in on-site molecule. However, in the case of mixed-valence complexes whose spin states are situated in the spin-crossover region, it is expected that new types of conjugated phenomena coupled with spin and charge take place between different metal ions in order to minimize the free energy in the whole system.

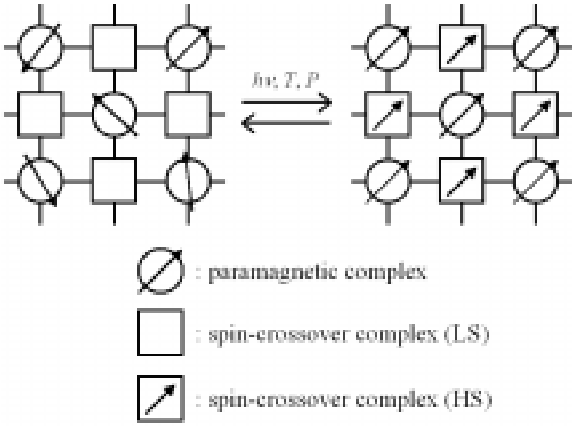

Fig. 1. Assembled hetero-metal complex system including spin-crossover complex ion. The spin crossover transition behaves as a switching function to control the magnetic interaction and the magnetic ordering in the assembled hetero-metal complex system

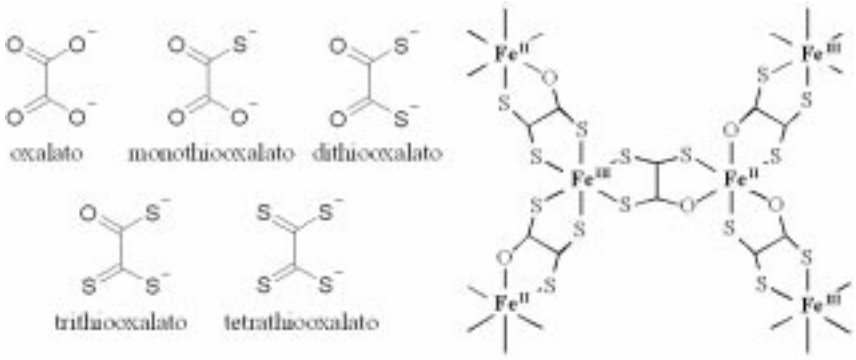

Fig. 2. Oxalato derivatives as bridging ligand, and the network structure of $[Fe^{II}Fe^{III}(tto)_3]$ complex

From these viewpoints, we have synthesized iron mixed-valence complexes whose spin states are situated in the spin-crossover region. It is well known that tris(dithiocarbamato)

iron(III) complexes show the spin-crossover transition [4]. In these complexes, Fe^{III} is co-ordinated by six S atoms. In the cases of $Fe^{III}O_6$ and $Fe^{II}O_6$ octahedra, on the other hand, there has been no report on the thermally induced spin-crossover transition at ambient pressure. Taking account of these iron complexes, we have systematically synthesized iron mixed valence complexes by using oxalato derivatives as bridging ligands, which is shown in Fig. 2. Recently, we have discovered a new type of phase transition coupled with spin and charge around 120 K for $(n\text{-}C_3H_7)_4N[Fe^{II}Fe^{III}(dto)_3]$[5,6].

In this paper, we report and discuss the spin-entropy driven charge-transfer phase transition in $(n\text{-}C_nH_{2n+1})_4N[Fe^{II}Fe^{III}(dto)_3]$(dto = dithiooxalato($C_2O_2S_2$)). Moreover, we put forward various multifunctional properties for $(n\text{-}C_nH_{2n+1})_4N[Fe^{II}Fe^{III}(mto)_3]$ (mto = monothiooxalato(C_2O_3S)) and $(n\text{-}C_nH_{2n+1})_4N[Fe^{II}Fe^{III}(tto)_3]$ (tto = trithiooxalato(C_2OS_3)).

2. Experimental

K_2(mto), K_2(dto) and K_2(tto) were synthesized in the similar way as reported in Ref. [7, 8]. $(n\text{-}C_nH_{2n+1})_4N[Fe^{II}Fe^{III}(dto)_3]$($n$ = 3–6) was synthesized in a similar way to prepare $(n\text{-}C_3H_7)_4N[M^{II}Cr^{III}(dto)_3]$(M = Fe, Co, Ni, Zn)[9]. A solution of KBa[Fe $(dto)_3]\cdot 6H_2O$[8] in a methanol–water mixture was stirred and a solution of $FeCl_2\cdot 4H_2O$ and $(n\text{-}C_nH_{2n+1})_4NBr$ in a methanol-water mixture was added. In this way, $(n\text{-}C_nH_{2n+1})_4N$ $[Fe^{II}Fe^{III}(dto)_3]$ was obtained as black coloured precipitate. In this similar way, $(n\text{-}C_nH_{2n+1})_4N[Fe^{II}Fe^{III}(mto)_3]$ and $(n\text{-}C_nH_{2n+1})_4N[Fe^{II}Fe^{III}(tto)_3]$ were synthesized.

The static magnetic susceptibility was measured by a Quantum Design MPMS5 SQUID susceptometer. Powdered sample of 10 mg was wrapped in polyethylene film and held in a plastic straw. The magnetic susceptibility obtained was corrected for the background and the core diamagnetism estimated from Pascal's constants. In the case of ^{57}Fe Mössbauer spectroscopic measurement, ^{57}Co in Rh was used at 298 K as a Mössbauer source. The spectra were calibrated by using the six lines of a body-centred cubic iron foil (α-Fe), the centre of which was taken as zero isomer shift. The hyperfine parameters were obtained by least-squares fitting to Lorentzian line shapes.

3. Results and discussion

The crystal structure of $(n\text{-}C_nH_{2n+1})_4N[Fe^{II}Fe^{III}(dto)_3]$ consists of two-dimensional honeycomb network structure, $[Fe^{II}Fe^{III}(dto)_3]_\infty$, and intercalated $(n\text{-}C_nH_{2n+1})_4N^+$ cations. Figure 3 shows the two-dimensional honeycomb network structure with alternating array of Fe^{II} and Fe^{III} atoms through dto bridges, and the alternation layer structure. At room temperature, the Fe^{III} (S = 1/2) and Fe^{II} (S = 2) sites are co-ordinated by six S atoms and six O atoms, respectively, which has been confirmed by means of ^{57}Fe Mössbauer spectroscopy. The space group is $P6_3$, consequently the conformations of the $Fe^{II}(O_2C_2S_2)_3$ and $Fe^{III}(S_2C_2O_2)_3$ octahedra in one $[Fe^{II}Fe^{III}(dto)_3]_\infty$ layer are different from those in the adja-

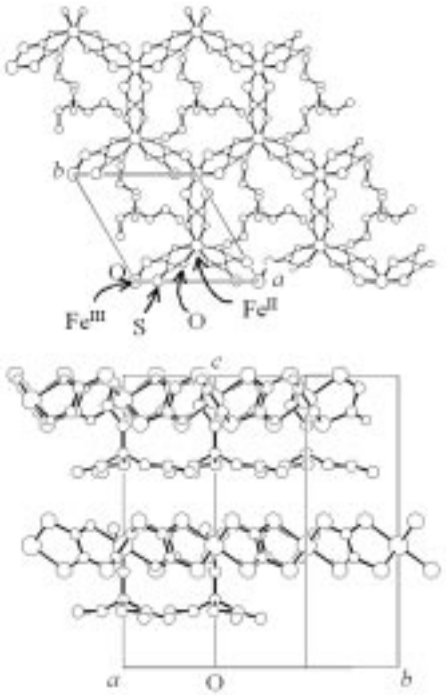

Fig. 3. Crystal structure of (n-$C_3H_7)_4N[Fe^{II}Fe^{III}(dto)_3]$ at 298 K

cent one $[Fe^{II}Fe^{III}(dto)_3]_\infty$ layer. One layer consists of Λ configuration of $Fe^{II}(O_2C_2S_2)_3$ and Δ configuration of $Fe^{III}(S_2C_2O_2)_3$, while the adjacent layer consists of Δ configuration of $Fe^{II}(O_2C_2S_2)_3$ and Λ configuration of $Fe^{III}(S_2C_2O_2)_3$. In $(n\text{-}C_nH_{2n+1})_4N^+$, the axial propyl chain points into the cavity of honeycomb network.

Figure 4 shows χT as a function of temperature for $(n\text{-}C_3H_7)_4N[Fe^{II}Fe^{III}(dto)_3]$. As shown in Fig. 4, χT increases with decreasing temperature except in the temperature region between 70 K and 130 K and shows a maximum around 10 K, which implies that the magnetic interaction between Fe^{II} and Fe^{III} in $(n\text{-}C_3H_7)_4N[Fe^{II}Fe^{III}(dto)_3]$ is ferromagnetic and the ferromagnetic transition takes place around 10 K. In fact, as shown in Fig. 4, the spontaneous magnetization appears at 7 K. The field cooled magnetization (FCM) under the external magnetic field of 30 G shows a rapid increase below 8 K and shows a tendency to saturate below 6 K. When the magnetic field is switched off at 1.8 K, the remnant magnetization (RM) remains, and vanishes at 7 K. The zero-field cooled magnetization (ZFCM) and FCM curves meet at 7 K where the magnetic hysteresis disappears. Consequently, the Curie temperature is estimated at 7 K.

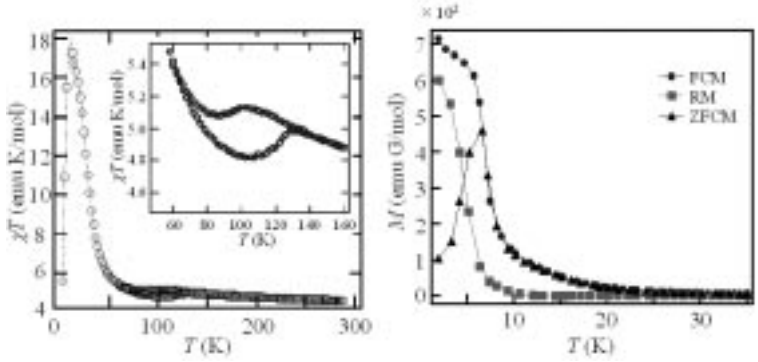

Fig. 4. Temperature dependence of χT under the external magnetic field of 5000 G and the temperature dependence of magnetization under the external magnetic field of 30 G for $(n\text{-}C_3H_7)_4N[Fe^{II}Fe^{III}(dto)_3]$. FCM, RM, and ZFCM denote the field-cooled magnetization, the remnant magnetization, and the zero-field cooled magnetization, respectively

Turning to χT vs. T curve in Fig.4, there is an anomalous drop with thermal hysteresis between 70 K and 130 K, which implies a first-order phase transition. In order to elucidate the detailed mechanism of the phase transition around 120 K, we investigated the ^{57}Fe Mössbauer spectra of $(n\text{-}C_3H_7)_4N[Fe^{II}Fe^{III}(dto)_3]$ at 105 K, 124 K and 130 K, which is shown in Fig. 5.

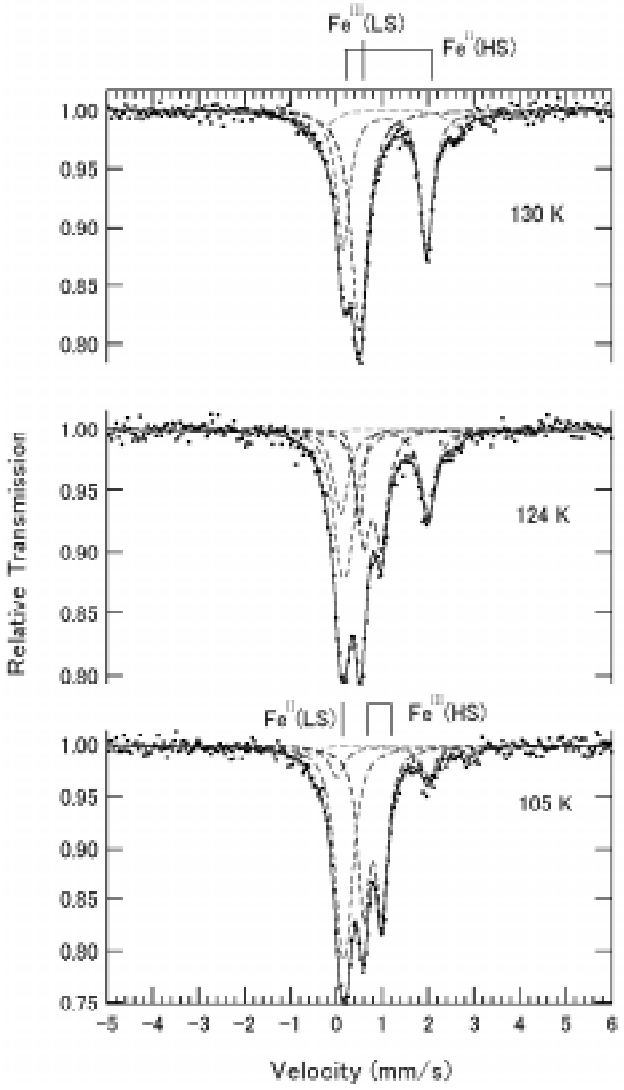

Fig. 5. ^{57}Fe Mössbauer spectra of $(n\text{-}C_3H_7)_4N[Fe^{II}Fe^{III}(dto)_3]$ at 130 K, 124 K and 105 K

At 130 K, the spectrum with two branches at 0.16 mm/s and 1.96 mm/s can be assigned to that for the high-spin state of the Fe^{II} site co-ordinated by six O atoms. The

isomer shift (*IS*) and the quadrupole splitting (*QS*) of the ^{57}Fe Mössbauer spectrum with two branches at 0.16 mm/s and 1.86 mm/s are estimated at 1.06 mm/s and 1.80 mm/s, respectively, whose values are quite similar to those (*IS* = 1.30 mm/s, *QS* = 1.79 mm/s at 78 K) of the ^{57}Fe Mössbauer spectrum for the Fe^{II}(*S* = 2) in $(n\text{-}C_4H_9)_4N[Fe^{II}Fe^{III}(ox)_3]$ [10], where the Fe^{II} site is co-ordinated by six O atoms. The spectrum with single peak at 0.46 mm/s can be assigned to that for the low-spin state of the Fe^{III} site co-ordinated by six S atoms. The *IS* and *QS* of the ^{57}Fe Mössbauer spectrum with single peak at 0.46 mm/s are quite similar to those (*IS* = 0.33 mm/s, *QS* = 0.35 mm/s at 196 K) of the ^{57}Fe Mössbauer spectrum for the Fe^{III}(*S* = 1/2) in $KBa[Fe^{III}(dto)_3]$, where the Fe^{III} is co-ordinated by six S atoms[11]. As shown in Fig. 5, with decreasing temperature, the line profile of ^{57}Fe Mössbauer spectra remarkably changes between 130 K and 105 K. At 105 K, the intensity of the spectrum corresponding to the Fe^{II} site decreases by 80% and new lines appear at about 0.2 mm/s and 1.0 mm/s, which implies a drastic change in the Fe electronic states of $(n\text{-}C_3H_7)_4N[Fe^{II}Fe^{III}(dto)_3]$ between 130 K and 105 K.

Comparing with the typical values of *IS* and *QS* of ^{57}Fe Mössbauer spectra for Fe^{II}(*S* = 0), Fe^{II}(*S* = 2), Fe^{III}(*S* = 1/2), and Fe^{III}(*S* = 5/2), the ^{57}Fe Mössbauer spectra of $(n\text{-}C_3H_7)_4N[Fe^{II}Fe^{III}(dto)_3]$ between 130 K and 105 K are assigned as shown in Fig. 5. In this way, from the analysis of ^{57}Fe Mössbauer spectra, we have discovered a new type of the first order phase transition around 120 K for $(n\text{-}C_nH_{2n+1})_4N[Fe^{II}Fe^{III}(dto)_3]$(*n* = 3, 4), where the charge-transfer transition between Fe^{II} and Fe^{III} occurs reversibly. In the higher temperature phase, the Fe^{III} (*S* = 1/2) and Fe^{II} (*S* = 2) sites are co-ordinated by six S atoms and six O atoms, respectively. In the lower temperature phase, on the other hand, the Fe^{III} (*S* = 5/2) and Fe^{II} (*S* = 0) sites are co-ordinated by six O atoms and six S atoms, respectively.

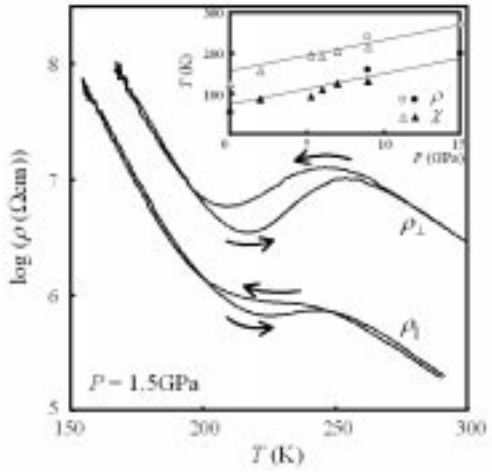

Fig. 6. Temperature dependence of the intra-layer ($\rho_{||}$) and inter-layer ($\rho_{\perp}$) resistivities of $(n\text{-}C_3H_7)_4N[Fe^{II}Fe^{III}(dto)_3]$ at 1.5 GPa. Arrows denote the direction of the thermal process. Inset shows the charge-transfer phase transition as a function of applied pressure determined by the magnetic susceptibility (χ) and the electrical resistivity (ρ) measurements. ○ Δ and ● ▲ denote the upper limit and the lower limit of the charge-transfer phase transition, respectively

In order to prove the charge-transfer phase transition in $(n\text{-}C_3H_7)_4N[Fe^{II}Fe^{III}(dto)_3]$, we have measured the electrical resistivity for the single crystal. Figure 6 shows the

temperature dependence of the intra-layer ($\rho_{||}$) and inter-layer ($\rho_{\perp}$) resistivity of (n-C_3H_7)$_4$N[$Fe^{II}Fe^{III}$ (dto)$_3$] at 1.5 GPa. The inset in Fig. 6 shows the critical temperature (T_c) of the charge-transfer phase transition as a function of applied pressure. At 1.5 GPa, the charge-transfer phase transition takes place between 200 K and 270 K. As shown in Fig. 6, both of the intra-layer and inter-layer resistivities show an anomalous drop due to the charge-transfer phase transition. The intra-layer resistivity is one order of magnitude lower than that of the inter-layer one, which is attributed to the electron hopping between Fe^{II} and Fe^{III} in the two-dimensional honeycomb network structure of [$Fe^{II}Fe^{III}$(dto)$_3$]$_\infty$.

Consequently, it is concluded that (n-C_nH_{2n+1})$_4$N[$Fe^{II}Fe^{III}$(dto)$_3$](n = 3, 4) undergoes a thermally induced charge-transfer phase transition coupled with the change of spin configuration around 120 K, where the charge-transfer transition occurs reversibly between the t_{2g} orbitals of the Fe^{II} and Fe^{III} sites, which is schematically shown in Fig. 7. The driving force responsible for the charge-transfer phase transition would be the difference in spin entropy between the higher and the lower temperature phases. It should be noted that the spin entropy in the higher temperature phase is Rln(2×5) = 19.15 J·K^{-1}·mol^{-1} and that in the lower temperature phase is Rln(1×6) = 14.90 J·K^{-1}·mol^{-1}, where R is the gas constant. Therefore, the spin-entropy gain expected from the charge transfer is estimated at 4.25 J·K^{-1}·mol^{-1}. Since the observed entropy gain at the charge-transfer phase transition in (n-C_3H_7)$_4$N[$Fe^{II}Fe^{III}$(dto)$_3$] is 9.20 J·K^{-1}·mol^{-1} [12], the entropy change originating in intra-molecular vibration is quite smaller than in normal spin-crossover transition. For example, about 35 J·K^{-1}·mol^{-1} was estimated for the vibrational contribution to the entropy change in the spin-crossover phenomenon observed in [Fe(phen)$_2$(NCS)$_2$] [13].

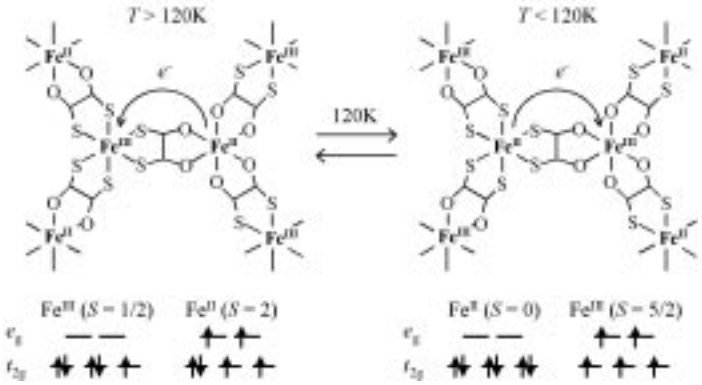

Fig. 7. Schematic representation of the charge-transfer phase transition around 120 K for (n-C_3H_7)$_4$N[$Fe^{II}Fe^{III}$(dto)$_3$]

The phase diagram of (n-C_nH_{2n+1})$_4$N[$Fe^{II}Fe^{III}$(dto)$_3$] is schematically shown in Fig. 8. The vertical axis denotes the free energy ($G = H - TS$). HTP and LTP denote the high-temperature phase with Fe^{II}(S = 2), Fe^{III}(S = 1/2) spin configuration and the

low-temperature phase with $Fe^{II}(S = 0)$, $Fe^{III}(S = 5/2)$ spin configuration, respectively. T_c is the transition temperature between HTP and LTP. The first-order phase transition around 120 K for $(n\text{-}C_nH_{2n+1})_4N[Fe^{II}Fe^{III}(dto)_3](n = 3, 4)$ is regarded as spin-entropy driven charge-transfer phase transition caused by minimizing the free energy in the whole system. As shown in Fig. 8, T_c strongly depends on the difference of enthalpy (ΔH) between HTP and LTP. With increasing ΔH, T_c presumably becomes to be higher. If the charge-transfer phase transition is of the first order without thermal hysteresis or of the second order, the hopping of Avogadro's number electrons would take place between the Fe^{II} and Fe^{III} sites, which would cause a spin-entropy driven metallization at T_c.

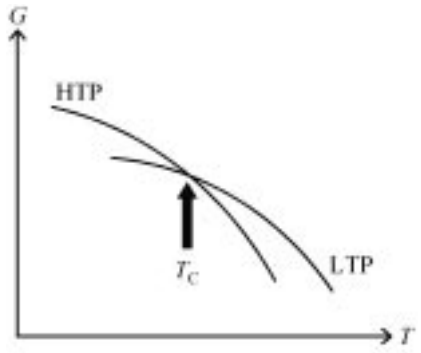

Fig. 8. Phase diagram of $(n\text{-}C_nH_{2n+1})_4N[Fe^{II}Fe^{III}(dto)_3]$. The vertical axis denotes the free enrgy ($G = H - TS$). HTP and LTP denote the high-temperature phase with $Fe^{II}(S = 2)$, $Fe^{III}(S = 1/2)$ spin configuration and the low-temperature phase with $Fe^{II}(S = 0)$, $Fe^{III}(S = 5/2)$ spin configuration, respectively. T_c denotes the transition temperature of the charge-transfer phase transition

Next, we discuss the mechanism of ferromagnetic ordering in $(n\text{-}C_nH_{2n+1})_4N[Fe^{II}Fe^{III}(dto)_3]$. As mentioned already, the spin states of the Fe^{II} and Fe^{III} sites in the lower temperature phase are the low-spin state ($S = 0$) and the high spin state ($S = 5/2$), respectively, where the super-exchange interaction through the sequence of Fe^{III}–(dto)–Fe^{II}–(dto)–Fe^{III} is considered to be negligibly small. The most plausible mechanism responsible for the ferromagnetic ordering at 7 K and 11 K for $(n\text{-}C_3H_7)_4N[Fe^{II}Fe^{III}(dto)_3]$ and $(n\text{-}C_4H_9)_4N[Fe^{II}Fe^{III}(dto)_3]$ is the charge-transfer interaction between the Fe^{II} and Fe^{III} sites. In the lower temperature phase of $(n\text{-}C_nH_{2n+1})_4N[Fe^{II}Fe^{III}(dto)_3](n = 3, 4)$, the ground state wave function perturbed by the charge-transfer interaction between the Fe^{II} and Fe^{III} sites is expressed as

$$\Psi = (1 - \alpha)^2\{\varphi_i(Fe^{II}(t_2{}^6))\varphi_j(Fe^{III}(t_2{}^3e^2))\} + \alpha\{\varphi_i(Fe^{III}(t_2{}^5))\varphi_j(Fe^{II}(t_2{}^4e^2))\}$$

where α denotes the degree of the charge-transfer interaction. Each Fe^{III} site in the lower temperature phase accepts a t_2 electron with down spin, because the t_2 and e orbitals in the Fe^{III} site are both exactly half occupied. Therefore, the spin configuration between Fe^{II} and Fe^{III} in the virtual state, $\varphi_i(Fe^{III}(t_2{}^5))\ \varphi_j(Fe^{II}(t_2{}^4e^2))$, is ferromagnetically coupled. In this way, the valence delocalization between the Fe^{II} ($S = 0$) and Fe^{III} ($S = 5/2$) sites induces the ferromagnetic ordering in the lower temperature phase of $(n\text{-}C_nH_{2n+1})_4N[Fe^{II}Fe^{III}(dto)_3]$ ($n = 3, 4$), which is the same mechanism of the ferromagnetic ordering ($T_c = 5.5$ K) in Prussian blue, $Fe^{III}{}_4[Fe^{II}(CN)_6]_3$[14, 15].

Finally, we propose the possibility of various multifunctional properties for n-$C_nH_{2n+1})_4N[Fe^{II}Fe^{III}(mto)_3]$ and $(n$-$C_nH_{2n+1})_4N[Fe^{II}Fe^{III}(tto)_3]$. These complexes have the possibility of large dielectric response and non-linear optical effect because the $Fe^{III}(SOC_2O_2)_3$ octahedra in $(n$-$C_nH_{2n+1})_4N[Fe^{II}Fe^{III}(mto)_3]$ and the $Fe^{II}(SOC_2S_2)_3$ octahedra in $(n$-$C_nH_{2n+1})_4N[Fe^{II}Fe^{III}(tto)_3]$ lose the inversion-symmetry. Consequently, the following multifunctional properties are expected for $(n$-$C_nH_{2n+1})_4N[Fe^{II}Fe^{III}X_3]$ (X = mto, dto, tto):

- spin-entropy driven insulator-to-metal transition at the charge-transfer phase transition,
- coexistence of ferromagnet and ferroelectrics,
- high T_c ferromagnets caused by charge-transfer interaction,
- non-linear optical effects induced by magnetic ordering,
- photo-induced magnetic ordering.

Acknowledgement

This work has been supported by a Grant-in-Aid for Scientific Research from the Ministry of Education, Culture, Sports, Science and Technology, Japan.

References

[1] DECURTINS S., GÜTLICH P., KÖHLER C.P., SPIERING H., HAUSER A., Chem. Phys. Lett., 105 (1984), 1.
[2] KRÖBER J., CODJOVI E., KAHN O., GROLIÈRE F., JAY C., J. Am. Chem. Soc., 115 (1993), 9810.
[3] KAHN O., MARTINEZ C.J., Science, 279 (1998), 44.
[4] CAMBI L., CAGNASSO A., Atti Accad. Naz. Lincei, 13 (1931), 809.
[5] KOJIMA N., AOKI W., SETO M., KOBAYASHI Y., MAEDA YU., Synth. Metals, 121 (2001), 1796.
[6] KOJIMA N., AOKI W., ITOI M., ONO Y., SETO M., KOBAYASHI Y., MAEDA YU, Solid State Commun., 120 (2001),165.
[7] STORK W., MATTES R., Angew. Chem. Int. Ed., 87 (1975), 452.
[8] LEITHEISER M., COUCOUVANIS D., J. Inorg. Nucl. Chem., 39 (1977), 811.
[9] ÔKAWA H., MITSUMI M., OHBA M., KODERA M., MATSUMOTO N., Bull. Chem. Soc. Jpn., 67 (1994), 2139.
[10] IIJIMA S., KATSURA T., TAMAKI H., MITSUMI M., MATSUMOTO N., ÔKAWA H., Mol. Cryst. Liq. Cryst., 233 (1993), 263.
[11] BIRCHALL T., TUN K.M., Inorg. Chem., 15 (1976), 376.
[12] NAKAMOTO T., MIYAZAKI Y., ITOI M., ONO Y., KOJIMA N., SORAI M., Angew. Chem. Int. Ed., 40 (2001), 4716.
[13] SORAI M., SEKI S., J. Phys. Chem. Solids, 35 (1974), 555.
[14] MAYOH B., DAY P., J. Chem. Soc. Dalton (1974), 846.
[15] MAYOH B., DAY P., J. Chem. Soc. Dalton. (1976), 1483.

Received 10 March 2003
Revised 26 March 2003